CRYSTAL GROWTH & DESIGN

Article

pubs.acs.org/crystal

Aspect-Ratio Controlled Synthesis and Tunable Luminescence of YF_3:Yb^{3+}/Er^{3+} Upconversion Nanocrystals

G. Murali,[†] R. K. Mishra,[†] Jae Myeong Lee,[†] Young Cheol Chae,[†] Jongwoo Kim,[‡] Yung Doug Suh,[‡] Dong-kwon Lim,*[,§] and Seung Hee Lee*[,†]

[†]Applied Materials Institute for BIN Convergence, Department of BIN Convergence Technology and Department of Polymer-Nano Science and Technology, Chonbuk National University, Jeonju, Jeonbuk 561-756, Korea

[‡]Laboratory for Advanced Molecular Probing (LAMP), Korea Research Institute of Chemical Technology, DaeJeon 305-600, South Korea

[§]KU-KIST Graduate School of Converging Science and Technology, Korea University, 145 Anam-ro, Seongbuk-gu, Seoul 136-701, Korea

S *Supporting Information*

ABSTRACT: We report a facile synthetic method for high-aspect-ratio YF_3:Yb^{3+}/Er^{3+} nanocrystals by controlling the composition of the precursor and salts to manipulate the structures of YF_3:Yb^{3+}/Er^{3+} nanocrystals. A controlled aspect ratio is attained by tuning the molar ratio of NH_4^+/RE^{3+} (NH_4^+ is the counterion released from the fluoride precursor (NH_4F) and RE^{3+} indicates the total amount of Y, Yb, and Er) and the presence of specific inorganic salts. A low molar ratio of NH_4^+/RE^{3+} induced the production of high-aspect-ratio YF_3:Yb^{3+}/Er^{3+} nanocrystals, while a high molar ratio of NH_4^+/RE^{3+} induced the formation of irregular nanoplates. The selection of the inorganic salt as an additive is critical in controlling the aspect ratio and crystallinity of YF_3:Yb^{3+}/Er^{3+} nanocrystals. The cation showed limited control over the aspect ratio, but the anions, Cl^- and Br^-, induced the production of the highest aspect ratio for YF_3:Yb^{3+}/Er^{3+} nanocrystals. We found that the aspect ratio affected the luminescence properties of YF_3:Yb^{3+}/Er^{3+} nanocrystals. The green emission from nanorod structures changed to orange when the morphology is transformed to nanoplates.

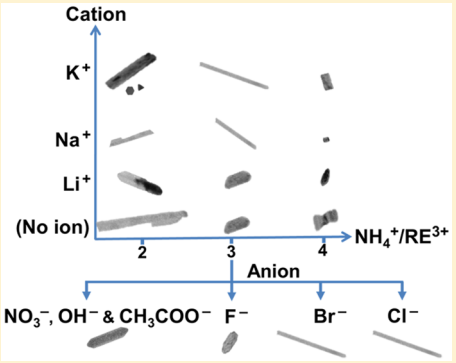

INTRODUCTION

Up-conversion (UC), an anti-Stokes emission process that converts higher-wavelength excitations into shorter-wavelength emissions, has inspired a new generation of research in many fields ranging from biomedical to display devices.[1−6] Material compositions that are commonly used for UC consists of a crystalline host and trivalent lanthanide ions as dopants (known as sensitizer and activator ions). The successful application of UC materials has depended upon their luminescent efficiency and emission wavelength. Generally, the selection of the host lattice and dopant ions is the key to tailor the luminescent efficiency and emission wavelength.[7−11] However, novel nanostructures also have significant potential to alter the optical properties of UC nanocrystals.[12−17]

To obtain a monodisperse and well-defined UC nanostructure, many synthetic procedures have been investigated using specific solvents, surfactants as structure-directing agents,[18−23] or specific counterions (i.e., K^+, H^+, NH_4^+, Na^+, Rb^+, and Cs^+) to prepare nanoplates, nanospheres, branched tree-like structures, nanobundles, nanorods, and nanowires, respectively.[24] Inorganic salt-assisted UC nanostructure synthesis has also been explored in terms of the role of inorganic species in the crystallization of UC nanostructures.[25,26] Ions can influence the growth rates of specific crystal facets, resulting in diverse morphologies of the final products.[27−31]

Rare-earth fluorides are being explored as UC host materials because of their low phonon energies, which favorably yield strong UC emissions by reducing the nonradiative loss.[32,33] YF_3 nano-/microstructures with unique morphologies have been synthesized with salt-assisted synthetic methods. For example, Fu et al.[34] synthesized truncated octahedral, walnut-like, and bundle-like morphologies of YF_3 by using inorganic salts such as NaCl, LiCl, KCl, and $BaCl_2$ as the structure-directing agent in the hydrothermal reaction. Qian et al.[35] demonstrated that the morphology of YF_3 could be controlled to be nanobones, nanospindles, nanoplates, and truncated and regular octahedra by controlling the reaction time and $NaNO_3$ concentration in the hydrothermal reaction. Recently, we found a synthetic method for nanoplate structures of YF_3:Yb^{3+}/Er^{3+} nanocrystals with strong luminescent properties by controlling the concentration of NaOH.[31] All these results indicate the complexity of controlling nanostructures of YF_3 UC nanocryst-

Received: December 10, 2016
Revised: March 18, 2017
Published: April 20, 2017

DOI: 10.1021/acs.cgd.6b01803
Cryst. Growth Des. 2017, 17, 3055−3061

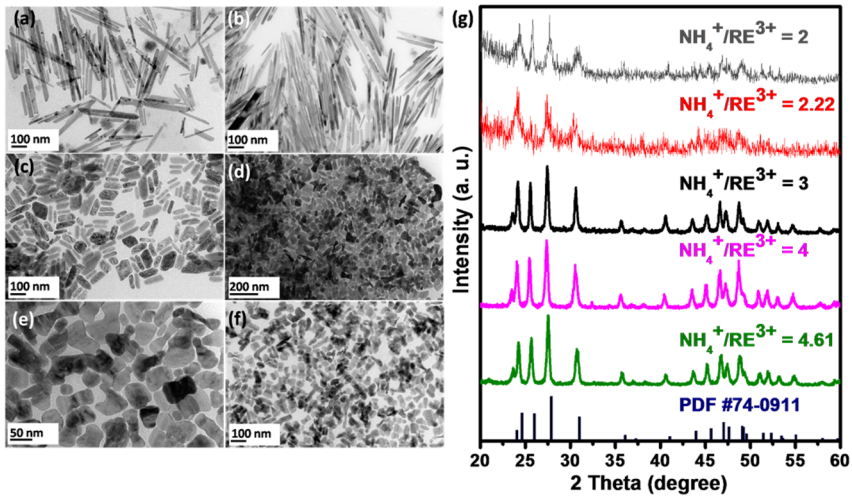

Figure 1. TEM images of YF_3:Yb^{3+}/Er^{3+} nanostructures synthesized using different NH_4^+/RE^{3+} molar concentrations: (a) 2, (b) 2.22, (c) 3, (d, e) 4, and (f) 4.61, (g) XRD patterns of YF_3:Yb^{3+}/Er^{3+} nanostructures.

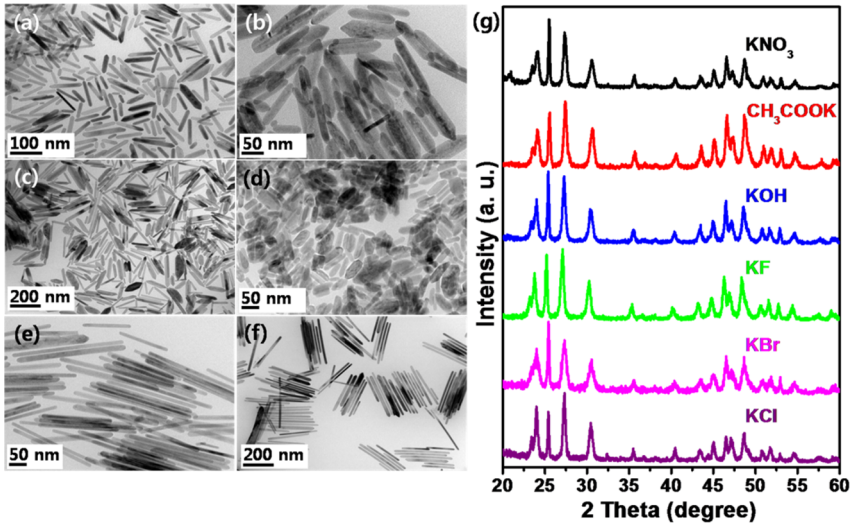

Figure 2. TEM images of YF_3:Yb^{3+}/Er^{3+} nanostructures prepared in the presence of (a) KNO_3, (b) CH_3COOK, (c) KOH, (d) KF, (e) KBr, and (f) KCl salts; (g) XRD patterns of prepared YF_3:Yb^{3+}/Er^{3+} nanostructures (NH_4^+/RE^{3+} = 3).

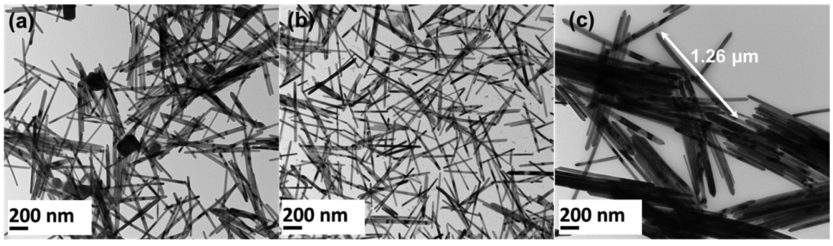

Figure 3. TEM images of YF_3:Yb^{3+}/Er^{3+} nanostructures prepared at NH_4^+/RE^{3+} = 3 in the presence of varying amounts of KCl: (a) 0.75 mmol and ODE/OM = 17:3, (b) 1.25 mmol and ODE/OM = 17:3, and (c) 1.25 mmol and ODE/OM = 15:5.

als, which requires systemic investigation to understand the detailed conditions related to the structural evolution of UC nanocrystals.

In this paper, we report a salt-controlled synthesis of high aspect-ratio YF_3:Yb^{3+}/Er^{3+} nanocrystals, which showed tunable emission intensity and emission colors from orange to green depending on the aspect ratio and shape. The aspect ratio and nanostructures of YF_3:Yb^{3+}/Er^{3+} nanocrystals were strongly dependent on the composition of the precursor and the types of ions of added inorganic salts.

MATERIALS AND METHODS

Materials. $YCl_3{\cdot}6H_2O$, $YbCl_3{\cdot}6H_2O$, $ErCl_3{\cdot}6H_2O$, NH_4F, KNO_3, CH_3COOK, KF, NaOH, LiOH, 1-octadecene (ODE), and oleylamine (OM) were purchased from Sigma-Aldrich (St. Louis, MO, USA). KCl was obtained from Shimakyu's Pure Chemicals (Osaka, Japan). KOH and NaCl were purchased from Showa Chemical Industry Co., Ltd. (Tokyo, Japan), while LiCl and KBr were supplied by Junsei Chemical

DOI: 10.1021/acs.cgd.6b01803
Cryst. Growth Des. 2017, 17, 3055−3061

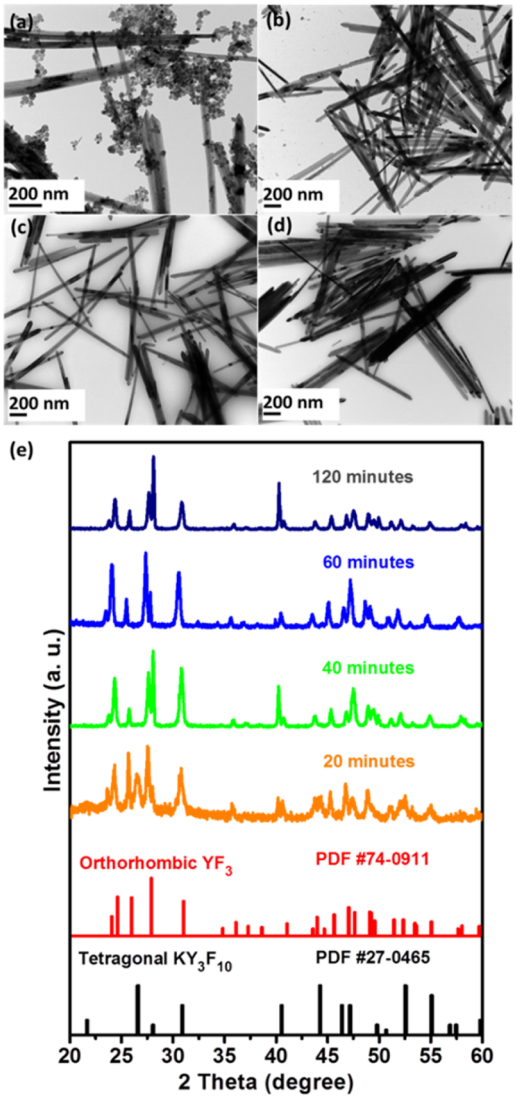

Figure 4. TEM images of YF_3:Yb^{3+}/Er^{3+} nanostructures prepared at NH_4^+/RE^{3+} = 3 in the presence of 1.25 mmol KCl and ODE/OM = 15:5 with (a) 20 min, (b) 40 min, (c) 60 min, and (d) 120 min reaction times. (e) XRD patterns of prepared YF_3:Yb^{3+}/Er^{3+} nanostructures.

Co., Ltd. (Tokyo, Japan) and Daejung Chemicals & Metals Co., Ltd. (Siheung-si, Gyonggi-do, Korea), respectively. All chemicals were used as received without further purification.

Typical Synthetic Procedures for YF_3:Yb^{3+}/Er^{3+} Nanostructures. Briefly, $YCl_3{\cdot}6H_2O$ (0.2366 g, 0.78 mmol), $YbCl_3{\cdot}6H_2O$ (0.0774 g, 0.20 mmol), and $ErCl_3{\cdot}6H_2O$ (0.0076 g, 0.02 mmol) were mixed with 3 mL of oleylamine (OM) and 17 mL of 1-octadecene (ODE) in a 50 mL round-bottom flask under continuous stirring. The mixture was heated to 160 °C to homogenize the solution and maintained at this temperature for 30 min. The mixture was then cooled to room temperature (25 °C), and 10 mL of a methanol solution containing NH_4F (0.1111 g, 3 mmol) was added dropwise. The mixed solution was stirred for 30 min. Then the solution was heated to 120 °C and maintained at this temperature for 15 min to remove excess methanol. Subsequently, the solution was heated to 310 °C and maintained at this temperature for 2 h under an Ar atmosphere. Afterward, the solution was naturally cooled to room temperature (25 °C). The nanocrystals were precipitated by centrifugation (5000 rpm, 5 min). Finally, the precipitates were washed twice with ethanol and dispersed in ethanol.[31] The effect of the precursor salt composition on the resulting YF_3:Yb^{3+}/Er^{3+} nanostructure was investigated by adjusting the NH_4^+/RE^{3+} (NH_4^+ = counterion released from fluoride precursor (NH_4F) and RE = total amount of Y, Yb, and Er) ratio from 2 to 2.22, 3, 4, and 4.61 (i.e., molar ratio of NH_4F to $RECl_3.6H_2O$ was adjusted from 2/1 to 3/1.35, 3/1, 4/1, 3/0.65, and 4/0.65, in which Y:Yb:Er was fixed to 78:20:2) while maintaining other experimental conditions at fixed values. To study the influence of anions and cations on YF_3:Yb^{3+}/Er^{3+} nanostructures, the selected inorganic salt (0.25 mmol) was introduced into the reaction medium in the NH_4F and methanol addition step.

Characterization. The crystallinity of the nanostructures was determined by X-ray powder diffraction (XRD) using a MAX-2500 instrument and Fe-filtered Cu−K_α radiation (λ = 1.54 Å). The products were characterized by high-resolution transmission electron microscopy (HRTEM) (HITACHI H-7650 and JEOL JEM-2010). The aspect-ratio of products was determined by measuring about 100 particles in the TEM images. Fluorescence spectra were recorded using a homemade microscope equipped with a spectrometer and a near-infrared (NIR) laser (980 nm).The solution of each sample was dropped into a silicone isolator (P24742, Thermo Fisher Scientific) on a cover glass and placed under a microscope (IX71, Olympus). The sample was irradiated by a 980 nm laser from a single-mode laser diode (AC1401-0600-980-SM, EM4) using an epifluorescence technique. The PL spectra were measured from the emitted beam passing through the microscope by a CCD camera (PIXIS400BR, Princeton Instruments) equipped with a spectrograph (SCT320, Princeton Instruments).

Results and Discussion. Effect of NH_4^+/RE^{3+} Ratio on Nanostructure of YF_3:Yb^{3+}/Er^{3+} Nanocrystals. The YF_3:Yb^{3+}/Er^{3+} nanocrystals were prepared with typical synthetic procedures but with varying NH_4^+/RE^{3+} ratios (2, 2.22, 3, 4, and 4.61). The TEM image showed high aspect-ratio YF_3:Yb^{3+}/Er^{3+} nanocrystals (length: 70−530 nm, width: 10−50 nm, aspect ratio: 13.7 ± 5.3 or 11.7 ± 4.8) prepared with a low NH_4^+/RE^{3+} molar ratio (2 or 2.22), as shown in Figure 1a,b and S1a,b in Supporting Information. When the NH_4^+/RE^{3+} ratio increased to 3, the aspect ratio of the nanocrystals decreased dramatically to 2.9 ± 0.7 (length: 50−155 nm, width: 22−55 nm) (Figures 1c and S1c). However, at molar ratios of NH_4^+/RE^{3+} of 4 or 4.61, irregular plate structures were dominantly obtained (length: 40−130 nm, width: 20−75 nm, aspect ratio: 1.9 ± 0.6 or 1.9 ± 0.5) (Figures 1d−f and S1d,e).

The XRD patterns of samples with different NH_4^+/RE^{3+} ratios are shown in Figure 1g. Although all samples showed the orthorhombic phase, peaks were well indexed to those of standard orthorhombic YF_3 according to PDF card no: PDF #74-0911. YF_3:Yb^{3+}/Er^{3+} nanocrystals with a high aspect ratio prepared with a low NH_4^+/RE^{3+} molar ratio (2 or 2.22) showed poor crystallinity in the XRD spectrum. HRTEM analysis revealed that the rod-shaped structure of YF_3:Yb^{3+}/Er^{3+} nanocrystals has extensive defect structures inside the nanorods, as shown in Figure S2a, which reduces the crystallinity of the structures. The number of internal defect structures decreased with increasing molar ratio of NH_4^+/RE^{3+} (Figure S2), which resulted in increased crystallinity of YF_3:Yb^{3+}/Er^{3+} nanocrystals.

The surface defect formation is closely associated with the shape, size, and aspect ratio of nanostructures.[36] Accordingly, morphologies with larger aspect ratios are prone to have higher defects.[36] Therefore, nanocrystals prepared at NH_4^+/RE^{3+} molar ratios of 2 and 2.22, which had larger aspect ratios compared to other structures, had larger defect structures, which eventually resulted in poor crystallization or XRD peaks. The high aspect ratios of YF_3:Yb^{3+}/Er^{3+} nanocrystals obtained using different precursor compositions have not been reported.

Role of Surfactant Composition. To examine the role of surfactants in the production of rod-shaped nanocrystals, we carried out the reactions (NH_4^+/RE^{3+} = 3) with varied solvent compositions, such as 100% OM, 1:1 mixture of ODE and OM, and 100% ODE solvent. The presence of OM in the solvent resulted in rod-shaped nanocrystals, and the structures turned out to be nonuniform at higher OM concentrations (Figures 1c and S3a,b). As shown in Figure S3c, 100% ODE solvent yielded mostly aggregated nanoparticles rather than nanorods, which indicates that the OM in the solvent promotes

DOI: 10.1021/acs.cgd.6b01803
Cryst. Growth Des. 2017, 17, 3055−3061

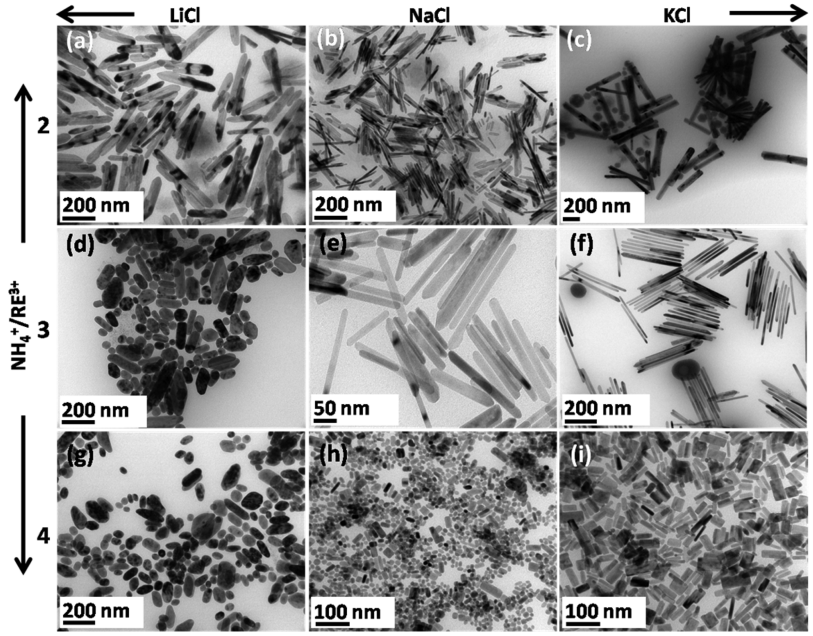

Figure 5. TEM images of YF_3:Yb^{3+}/Er^{3+} nanostructures prepared in the presence of LiCl, NaCl, and KCl salts at NH_4^+/RE^{3+} ratios of (a–c) 2, (d–f) 3, and (g–i) 4.

the anisotropic one-dimensional growth of YF_3:Yb^{3+}/Er^{3+} nanocrystals (Figure S3).

It is expected that the NH_4^+ ions affect the YF_3 crystal growth in two ways. First, a layer of NH_4^+ ions around the growing YF_3 crystals reduces the nucleation of crystals by resisting the diffusion of the growth-required ions from the solution into the grain.[37,25] Therefore, a higher concentration of NH_4^+ ions in the precursor solution leads to the formation of smaller size crystals, while, at a lower concentration of NH_4^+, larger crystals are produced. Second, because of the typical zirconium-type structure of YF_3, which is formed through the stacking of YF_8 units, NH_4^+ ions selectively attack different crystallographic planes and alter their growth.[35] Different NH_4^+ contents involved in each NH_4^+/RE^{3+} ratio condition modify the relative growth of crystal planes accordingly, causing the formation of nanocrystals with different shapes. Therefore, the variation in the NH_4^+ ion concentration associated with the NH_4^+/RE^{3+} molar ratio significantly affects the growth rate and anisotropic growth of YF_3 crystals and leads to the formation of morphologies with different sizes and shapes, as displayed in Figure 1a–f.

Effect of Anions on the Morphology of YF_3: Yb^{3+}/Er^{3+} Nanostructures. To elucidate the influence of anions on the resulting YF_3: Yb^{3+}/Er^{3+} nanostructure, samples were prepared by adding 0.25 mmol of a series potassium salts (KNO_3, CH_3COOK, KOH, KF, KBr, and KCl). (The molar ratio of NH_4^+/RE^{3+} was fixed to 3.0.) (Figure 2).

The TEM analysis shows that the addition of KNO_3, CH_3COOK, KOH, and KF salts showed no significant changes in the aspect ratio and morphology of nanocrystals (Figure 2a–d). Although the aspect ratios of nanocrystals were in the ranges of 4.7 ± 1.6, 4.0 ± 0.9, 5.9 ± 2.6, and 2.7 ± 0.7 for KNO_3, CH_3COOK, KOH, and KF, respectively (Figure S4a–d), most morphologies were similar to that obtained in the absence of salt (Figure 1c). On the contrary, the addition of KBr or KCl salts induced a great increase in the aspect ratio (Figure 2e,f). The aspect ratios were in the range of 18.8 ± 5.4 and 17.5 ± 5.5, respectively (Figure S4e,f) (The detailed dimensions are summarized in Table S1). More importantly, XRD patterns of all prepared products revealed the pure orthorhombic YF_3 phase with no significant defects (Figure 2g). Despite their high aspect ratios, nanocrystals prepared using KBr and KCl exhibited strong and sharp diffraction peaks, demonstrating the reduced defect structure with the use of Br^- and Cl^- ions. The results are consistent with the results reported by Pileni and co-workers. Among SO_4^{2-}, CO_3^{2-}, Cl^-, Br^-, NO_3^-, and ClO_4^- counterions released from Na^+ cations, only Cl^- and Br^- anions are capable of tuning the growth of copper particles and producing nanorods and mixtures of cubes and nanorods, respectively.[38] Further, The elemental mapping profiles and EDX analysis for the nanorod prepared with KCl salt shown in Figure S5 indicate that the K^+ and Cl^- ions released from the KCl salt are not entered into the crystal lattice of final YF_3: Yb^{3+}/Er^{3+} products. When the concentration of KCl was increased from 0.25 to 0.75 and 1.25 mmol, the aspect ratio of nanocrystals further increased from 17.5 ± 5.5 to 22.8 ± 5.1 and 20.0 ± 3.9 (Figures 3a,b and S6a,b), respectively. The tuning of solvent composition ODE/OM to 15:5 at a concentration of 1.25 mmol KCl resulted in 24.5 ± 6.0 aspect ratio with micrometer length of dimensions of the nanocrystals (Figures 3c and S6c). In spite of high aspect-ratio of nanocrystals synthesized from high KCl concentrations, Figure S7 displays predominant orthorhombic YF_3 crystal structure of nanocrystals.

To understand the growth process of high aspect-ratio YF_3:Yb^{3+}/Er^{3+} nanocrystals (ODE/OM is 15:5 at 1.25 mmol KCl), aliquots are taken at 20, 40, and 60 min reaction times during the reaction and analyzed using XRD and TEM (Figure 4). Initially, after 20 min of reaction, a spherical particle morphology is formed, and it has the dominant orthorhombic YF_3 crystalline phase with a noticeable proportion of the tetragonal KY_3F_{10} phase (Figure 4e). In addition, the formation of one-dimensional nanocrystals through Ostwald ripening of spherical particles was observed (Figures 4a and S8). As evidenced by the TEM images, continued growth resulted in a decrease in the fraction of spherical-shaped particles relative to the amount of nanorods (Figure 4a–d). After 60 min, only nanorods are observed (Figure 4c,d). This development confirmed that Ostwald ripening of spherical particles certainly contributed to the growth of nanorods. The XRD patterns indicate that the prolonged reaction improved the purity of the dominant orthorhombic YF_3 phase (Figure 4e).

Effect of Cations on the YF_3:Yb^{3+}/Er^{3+} Nanostructure. Potassium salt mostly induced the formation of rod-shaped nanostructures, and the dependence of the cation on the resulting nanostructures is of great importance in understanding the mechanism of shape evolution. To understand the role of the cation, we performed reactions in the presence of LiCl, NaCl, and KCl (0.25 mmol) at NH_4^+/RE^{3+} molar ratios of 2, 3, and 4 (Figures 5 and S8). All salts produced nanocrystals with a predominant orthorhombic YF_3 crystalline phase (Figure S9). At a NH_4^+/RE^{3+} ratio of 2, all salts resulted in a nanorod morphology (Figure 5a–c). However, when the

DOI: 10.1021/acs.cgd.6b01803
Cryst. Growth Des. 2017, 17, 3055–3061

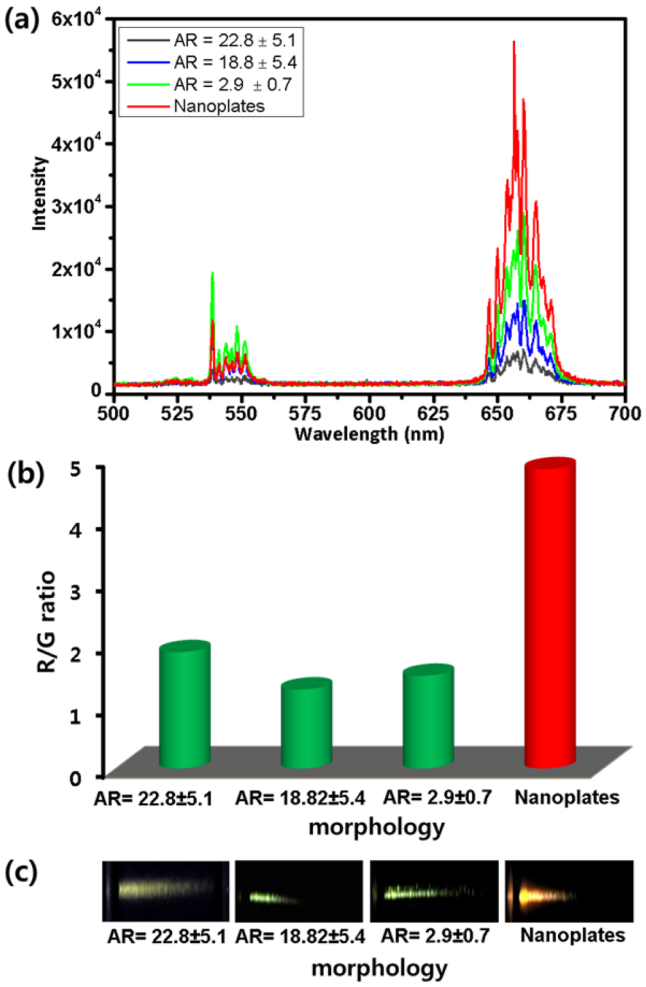

Figure 6. (a) Photoluminescence spectra, (b) red-to-green emission ratio, and (c) photoluminescence images of nanorods with different aspect ratios (AR = 22.8 ± 5.1, 18.8 ± 5.4, and 2.9 ± 0.7) and nanoplates. The aspect ratio of nanorods was controlled to be 22.8 ± 5.1, 18.8 ± 5.4, and 2.9 ± 0.7 using KCl = 0.75 mmol, KBr = 0.25 mmol, and the absence of salt, respectively, at NH_4^+/RE^{3+} = 3. Nanoplates were synthesized at NH_4^+/RE^{3+} = 4.61.

NH_4^+/RE^{3+} ratio was increased to 3 and then to 4, the dimensions of the nanocrystals decreased significantly for all salts (Figure 5d–i). This trend correlates with the significant role of the NH_4^+/RE^{3+} ratio in controlling the size of the nanocrystals. At a NH_4^+/RE^{3+} ratio of 3, Na^+ and K^+, while at a NH_4^+/RE^{3+} ratio of 4, only K^+ ions could produce the nanorods shape morphology (Figure 5e,f,i).

After the addition of inorganic salts, at the initial stage of reactions, cations are selectively absorbed on various crystalline facets of the initially formed YF_3 nucleation seeds due to the strong interactions between the cations and F^- anions on the surface of the nuclei; on the other hand, the anions (OH^-, CH_3COO^-, NO_3^-, Cl^-, and Br^-) are coordinated by different modes and coordination strengths with the existing cations. Owing to dissimilar size of cations (Li^+, Na^+, and K^+), crystallographic facets show different interaction strengths to different cations. Therefore, the number of cations absorbed on the crystal facets of budding YF_3 nucleation seeds is possibly different. This affects the relative growth rates of crystal facets and leads to the formation of products with different sizes. Ions influence is more effective in longitudinal growth as the lateral growth is restricted by OM. The tendency to form the nanorod morphology increases with an increase in the cation radius [Li^+ (60 pm) < Na^+ (95 pm) < K^+ (133 pm)].[39]

All these results demonstrate that the precursor composition and the specific inorganic salt should be selected carefully to finely control the morphologies of YF_3:Yb^{3+}/Er^{3+} nanocrystals. The diversity in the morphology can be attributed to the combined effects of cations (Na^+, K^+, Li^+, and NH_4^+ ions) and anions.

Photoluminescence. UC photoluminescence (PL) spectra of samples with different aspect ratios (22.8 ± 5.1, 18.8 ± 5.4 and 2.9 ± 0.7) and nanoplates were acquired under the excitation of a 980 nm wavelength laser. PL spectra of samples consisted of green (536–560 nm) and red (645–680 nm) emission bands, as shown in Figure 6a. Green and red emission bands are attributed to Er transitions from $^4S_{3/2}$ to $^4I_{15/2}$ and $^4F_{9/2}$ to $^4I_{15/2}$, respectively. Although the positions of these emission bands are identical for all samples, the relative intensities of each emission peak are different. The emission intensity ranging from 645–680 nm, corresponding to red, gradually decreased with the increase of the aspect ratio, as shown in Figure 6a, but the emission intensity ranging from 536–560 nm increased slightly with the increase in the aspect ratio, except for AR = 22.8 ± 5.1. The calculated red-to-green emission intensity ratio (R/G ratio) was found to be 2.0 for AR = 22.8 ± 5.1, 1.7 for AR = 18.8 ± 5.4, 1.8 for AR = 2.9 ± 0.7, and 5.0 for nanoplates (Figure 6b). For this reason, the excited solution colors of the samples with 980 nm laser were found to be yellowish green, green, green, and orange for AR = 22.8 ± 5.1, AR = 18.8 ± 5.4, AR = 2.9 ± 0.7, and nanoplates, respectively (Figure 6c).

CONCLUSION

In summary, we report a novel approach to finely control the aspect ratio of YF_3:Yb^{3+}/Er^{3+} nanocrystals by tailoring the precursor composition and adding inorganic salts to the reaction medium. The nanocrystals were fabricated from nanorods into nanoplates simply by the adjustment of NH_4^+/RE^{3+} mole ratio in the range of 2–4.61. Furthermore, the aspect ratio of nanocrystals was well controlled by the addition of inorganic salts. Br^- and Cl^- anions are favorable to obtain nanocrystals with highest aspect ratio. When the added cation radius increased from Li^+ to K^+, the tendency to produce the nanorod morphology increased. Interestingly, the emission colors of nanocrystals were strongly dependent on the aspect-ratio. Nanorod structures exhibited green emission while nanoplate structures showed orange emission. Given the significant controllability of the morphology and luminescence, our synthesis method may contribute to progressive YF_3:Yb^{3+}/Er^{3+} UCNPs synthesis methods. In addition, the bright green and orange color emissions from the prepared YF_3:Yb^{3+}/Er^{3+} structures have promising applications in color displays, bioimaging, optical communication, efficient energy harvesting, and photocatalysis.

ASSOCIATED CONTENT

Supporting Information

The Supporting Information is available free of charge on the ACS Publications website at DOI: 10.1021/acs.cgd.6b01803.

Synthesis method for nanorods at higher KCl concentrations. HRTEM, SAED, XRD, elemental mapping and EDX data, and aspect ratio histograms of nanocrystals prepared at different compositions of solvent, NH_4^+/RE^{3+}, and salts (PDF)

AUTHOR INFORMATION

Corresponding Authors

*(D.-k.L.) E-mail: dklim@korea.ac.kr.
*(S.H.L.) E-mail: lsh1@chonbuk.ac.kr.

ORCID

Dong-kwon Lim: 0000-0001-6755-7477

Notes

The authors declare no competing financial interest.

DOI: 10.1021/acs.cgd.6b01803
Cryst. Growth Des. 2017, 17, 3055–3061

■ ACKNOWLEDGMENTS

This research was supported by the National Research Foundation of Korea (NRF) funded by the Ministry of Education (NRF-2016R1A2B3013825), KU-KIST school project. This research was also supported by "Research Base Construction Fund Support Program" funded by Chonbuk National University in 2017.

■ REFERENCES

(1) Gai, S.; Li, C.; Yang, P.; Lin, J. Recent Progress in Rare Earth Micro/Nanocrystals: Soft Chemical Synthesis, Luminescent Properties, and Biomedical Applications. *Chem. Rev.* **2014**, *114*, 2343−2389.
(2) Shen, J.; Sun, L. D.; Yan, C. H. Luminescent Rare Earth Nanomaterials for Bioprobe Applications. *Dalton Trans.* **2008**, 5687−5697.
(3) Li, X.; Zhang, F.; Zhao, D. Highly Efficient Lanthanide Upconverting Nanomaterials: Progresses and Challenges. *Nano Today* **2013**, *8*, 643−676.
(4) Huang, X.; Han, S.; Huang, W.; Liu, X. Enhancing Solar Cell Efficiency: The Search for Luminescent Materials as Spectral Converters. *Chem. Soc. Rev.* **2013**, *42*, 173−201.
(5) deBettencourt-Dias, A. Lanthanide-based Emitting Materials in Light-emitting Diodes. *Dalton Trans.* **2007**, 2229−2241.
(6) Downing, E.; Hesselink, L.; Ralston, J.; Macfarlane, R. A. Three-Color, Solid-State, Three-Dimensional Display. *Science* **1996**, *273*, 1185−1189.
(7) Ehlert, O.; Thomann, R.; Darbandi, M.; Nann, T. A. Four-Color Colloidal Multiplexing Nanoparticle System. *ACS Nano* **2008**, *2*, 120−124.
(8) Yi, G. S.; Chow, G. M. Synthesis of Hexagonal-Phase $NaYF_4$:Yb,Er and $NaYF_4$:Yb,Tm Nanocrystals with Efficient Up-Conversion Fluorescence. *Adv. Funct. Mater.* **2006**, *16*, 2324−2329.
(9) Li, F.; Li, C.; Liu, X.; Chen, Y.; Bai, T.; Wang, L.; Shi, Z.; Feng, S. Hydrophilic, Upconverting, Multicolor, Lanthanide-Doped $NaGdF_4$ Nanocrystals as Potential Multifunctional Bioprobes. *Chem. - Eur. J.* **2012**, *18*, 11641−11646.
(10) Chen, G.; Qiu, H.; Fan, R.; Hao, S.; Tan, S.; Yang, C.; Han, G. Lanthanide-doped Ultra-small Yttrium Fluoride Nanoparticles with Enhanced Multicolor Upconversion Photoluminescence. *J. Mater. Chem.* **2012**, *22*, 20190−20196.
(11) Qiu, H.; Chen, G.; Sun, L.; Hao, S.; Han, G.; Yang, C. Ethylenediamine Tetraacetic Acid (EDTA)-controlled Synthesis of Multicolor Lanthanide Doped $BaYF_5$ Upconversion Nanocrystals. *J. Mater. Chem.* **2011**, *21*, 17202−17208.
(12) Wang, F.; Liu, X. Upconversion Multicolor Fine-Tuning: Visible to Near-Infrared Emission from Lanthanide-Doped $NaYF_4$ Nanoparticles. *J. Am. Chem. Soc.* **2008**, *130*, 5642−5643.
(13) Wang, Y.; Cai, R.; Liu, Z. Controlled Synthesis of $NaYF_4$: Yb, Er Nanocrystals with Upconversion Fluorescence *via* a Facile Hydrothermal Procedure in Aqueous Solution. *CrystEngComm* **2011**, *13*, 1772−1774.
(14) Quintanilla, M.; Nunez, N. O.; Cantelar, E.; Ocana, M.; Cusso, F. Tuning from Blue to Magenta the Up-converted Emissions of YF_3:Tm^{3+}/Yb^{3+} Nanocrystals. *Nanoscale* **2011**, *3*, 1046−1052.
(15) Qiu, H.; Chen, G.; Fan, R.; Yang, L.; Liu, C.; Hao, S.; Sailor, M. J.; Agren, H.; Yang, C.; Prasad, P. N. Intense Ultraviolet Upconversion Emission from Water-dispersed Colloidal YF_3:Yb^{3+}/Tm^{3+} Rhombic Nanodisks. *Nanoscale* **2014**, *6*, 753−757.
(16) Saboktakin, M.; Ye, X.; Chettiar, U. K.; Engheta, N.; Murray, C. B.; Kagan, C. R. Plasmonic Enhancement of Nanophosphor Upconversion Luminescence in Au Nanohole Arrays. *ACS Nano* **2013**, *7*, 7186−7192.
(17) Dyck, N. C.; van Veggel, F. C. J. M.; Demopoulos, G. P. Size-Dependent Maximization of Upconversion Efficiency of Citrate-Stabilized β-phase $NaYF_4$:Yb^{3+},Er^{3+} Crystals via Annealing. *ACS Appl. Mater. Interfaces* **2013**, *5*, 11661−11667.
(18) Shan, J.; Ju, Y. A Single-step Synthesis and the Kinetic Mechanism for Monodisperse and Hexagonal-phase NaYF4:Yb,Er Upconversion Nanophosphors. *Nanotechnology* **2009**, *20*, 275603.
(19) Shi, F.; Wang, J.; Zhang, D.; Qin, G.; Qin, W. Greatly Enhanced Size-tunable Ultraviolet Upconversion Luminescence of Monodisperse β-NaYF4:Yb,Tm Nanocrystals. *J. Mater. Chem.* **2011**, *21*, 13413−13421.
(20) Du, Y. P.; Zhang, Y. W.; Sun, L. D.; Yan, C. H. Optically Active Uniform Potassium and Lithium Rare Earth Fluoride Nanocrystals Derived from Metal Trifluroacetate Precursors. *Dalton Trans.* **2009**, 8574−8581.
(21) Du, Y. P.; Sun, X.; Zhang, Y. W.; Yan, Z. G.; Sun, L. D.; Yan, C. H. Uniform Alkaline Earth Fluoride Nanocrystals with Diverse Shapes Grown from Thermolysis of Metal Trifluoroacetates in Hot Surfactant Solutions. *Cryst. Growth Des.* **2009**, *9*, 2013−2019.
(22) Liu, C.; Sun, J.; Wang, H.; Chen, D. Size and Morphology Controllable Synthesis of Oil-dispersible LaF_3:Yb,Er Upconversion Fluorescent Nanocrystals via a Solid−liquid Two-phase Approach. *Scr. Mater.* **2008**, *58*, 89−92.
(23) Sun, X.; Zhang, Y. W.; Du, Y. P.; Yan, Z. G.; Si, R.; You, L. P.; Yan, C. H. From Trifluoroacetate Complex Precursors to Monodisperse Rare-Earth Fluoride and Oxyfluoride Nanocrystals with Diverse Shapes through Controlled Fluorination in Solution Phase. *Chem. - Eur. J.* **2007**, *13*, 2320.
(24) Wang, M.; Huang, Q. L.; Hong, J. M.; Chen, X. T.; Xue, Z. L. Controlled Synthesis and Characterization of Nanostructured EuF_3 with Different Crystalline Phases and Morphologies. *Cryst. Growth Des.* **2006**, *6*, 2169−2173.
(25) Zhao, Q.; Lü, W.; Guo, N.; Jia, Y.; Lv, W.; Shao, B.; Jiao, M.; You, H. Inorganic-salt-induced Morphological Transformation and Luminescent Performance of GdF_3 Nanostructures. *Dalton Trans.* **2013**, *42*, 6902−6908.
(26) Xue, X.; Wang, L.; Huang, L.; Zhao, D.; Qin, W. Effect of Alkali Ions on the Formation of Rare Earth Fluoride by Hydrothermal synthesis: Structure Tuning and Size Controlling. *CrystEngComm* **2013**, *15*, 2897−2903.
(27) Guria, A. K.; Pradhan, N. Doped or Not Doped: Ionic Impurities for Influencing the Phase and Growth of Semiconductor Nanocrystals. *Chem. Mater.* **2016**, *28*, 5224−5237.
(28) Wu, Q.; Zhang, F.; Xiao, P.; Tao, H.; Wang, X.; Hu, Z.; Lu, Y. Great Influence of Anions for Controllable Synthesis of CeO_2 Nanostructures: From Nanorods to Nanocubes. *J. Phys. Chem. C* **2008**, *112*, 17076−17080.
(29) Zhuang, T. T.; Yu, P.; Fan, F. J.; Wu, L.; Liu, X. J.; Yu, S. H. Controlled Synthesis of Kinked Ultrathin ZnSNanorods/Nanowires Triggered by Chloride Ions: A Case Study. *Small* **2014**, *10*, 1394−1402.
(30) Khodashenas, B.; Ghorbani, H. R. Synthesis of Silver Nanoparticles with Different Shapes. *Arabian J. Chem.* **2015**, DOI: 10.1016/j.arabjc.2014.12.014.
(31) Murali, G.; Lee, B. H.; Mishra, R. K.; Lee, J. M.; Nam, S. H.; Suh, Y. D.; Lim, D. K.; Lee, J. H.; Lee, S. H. Synthesis, Luminescence Properties, And Growth Mechanisms Of YF_3:Yb^{3+}/Er^{3+} Nanoplates. *J. Mater. Chem. C* **2015**, *3*, 10107−10113.
(32) Mai, H. X.; Zhang, Y. W.; Sun, L. D.; Yan, C. H. Highly Efficient Multicolor Up-Conversion Emissions and Their Mechanisms of Monodisperse $NaYF_4$:Yb,Er Core and Core/Shell-Structured Nanocrystals. *J. Phys. Chem. C* **2007**, *111*, 13721−13729.
(33) Mai, H. X.; Zhang, Y. W.; Si, R.; Yan, Z. G.; Sun, L. D.; You, L. P.; Yan, C. H. High-Quality Sodium Rare-Earth Fluoride Nanocrystals: Controlled Synthesis and Optical Properties. *J. Am. Chem. Soc.* **2006**, *128*, 6426−6436.
(34) Fu, Z.; Cui, X.; Cui, S.; Qi, X.; Zhou, S.; Zhang, S.; Jeong, J. H. Uniform Eu^{3+}-doped YF_3 Microcrystals: Inorganic Salt-Controlled Synthesis and their Luminescent Properties. *CrystEngComm* **2012**, *14*, 3915−3922.
(35) Qian, L.; Zai, J.; Chen, Z.; Zhu, J.; Yuan, Y.; Qian, X. Control of the Morphology and Composition of Yttrium Fluoride *via* a Salt-assisted Hydrothermal Method. *CrystEngComm* **2010**, *12*, 199−206.

DOI: 10.1021/acs.cgd.6b01803
Cryst. Growth Des. 2017, 17, 3055−3061

(36) Murali, G.; Reddy, D. A.; Sambasivam, S.; Giribabu, G.; Vijayalakshmi, R. P.; Venugopal, R.; Reddy, B. K. Morphology Dependent Luminescence from CdS Nanostructures. *Mater. Lett.* **2013**, *93*, 149−152.
(37) Liu, B.; Aydil, E. S. Growth of Oriented Single-Crystalline Rutile TiO_2 Nanorods on Transparent Conducting Substrates for Dye-Sensitized Solar Cells. *J. Am. Chem. Soc.* **2009**, *131*, 3985−3990.
(38) Filankembo, A.; Giorgio, S.; Lisiecki, I.; Pileni, M. P. Is the Anion the Major Parameter in the Shape Control of Nanocrystals. *J. Phys. Chem. B* **2003**, *107*, 7492−7500.
(39) Pauling, L. *The Nature of the Chemical Bond*, 3rd ed.; Cornell University Press: Ithaca, NY, 1960.

DOI: 10.1021/acs.cgd.6b01803
Cryst. Growth Des. 2017, 17, 3055−3061